Published in final edited form as:
Neuroimage. 2010 January 15; 49(2): 1350–1356. doi:10.1016/j.neuroimage.2009.09.060.

In Vivo Detection of Individual Glomeruli in the Rodent Olfactory Bulb Using Manganese Enhanced MRI

Kai-Hsiang Chuang[1], **Leonardo Belluscio**[2], and **Alan P. Koretsky**[1]

[1] Laboratory of Functional and Molecular Imaging, National Institutes of Health, Bethesda, MD 20892, USA

[2] Developmental Neural Plasticity Unit, National Institute of Neurological Disorders and Stroke, National Institutes of Health, Bethesda, MD 20892, USA

Abstract

MRI contrast based on relaxation times, proton density, or signal phase have been applied to delineate neural structures in the brain. However, neural units such as cortical layers and columns have been difficult to identify using these methods. Manganese ion delivered either systemically or injected directly has been shown to accumulate specifically within cellular areas of the brain enabling the differentiation of layers within the hippocampus, cortex, cerebellum, and olfactory bulb *in vivo*. Here we show the ability to detect individual olfactory glomeruli using manganese enhanced MRI (MEMRI). Glomeruli are anatomically distinct structures (~150 μm in diameter) on the surface of the olfactory bulb that represent the first processing units for olfactory sensory information. Following systemic delivery of $MnCl_2$ we used 3D-MRI with 50μm isotropic resolution to detect discrete spots of increased signal intensity between 100–200 μm in diameter in the glomerular layer of the rat olfactory bulb. Inflow effects of arterial blood and susceptibility effects of venous blood were suppressed and were evaluated by comparing the location of vessels in the bulb to areas of manganese enhancement using iron oxide to increase vessel contrast. These potential vascular effects did not explain the contrast detected. Nissl staining of individual glomeruli were also compared to MEMRI images from the same animals clearly demonstrating that many of the manganese enhanced regions corresponded to individual olfactory glomeruli. Thus, MEMRI can be used as a non-invasive means to detect olfactory glomeruli for longitudinal studies looking at neural plasticity during olfactory development or possible degeneration associated with disease.

Keywords

olfactory glomerulus; magnetic resonance imaging; neuroanatomy; molecular imaging

Introduction

Identification and quantification of neuroanatomical changes are important for understanding brain development and evaluating the progression of disease. Although MRI provides excellent

*Correspondence to: Kai-Hsiang Chuang, Ph.D., Laboratory of Molecular Imaging, Singapore Bioimaging Consortium, 11 Biopolis Way, #02-02, Singapore 138667, Phone: +65-64788764, chuang_kai_hsiang@sbic.a-star.edu.sg.

part of the results had been presented in the International Society for Magnetic Resonance in Medicine 15th Scientific Meeting & Exhibition, Berlin, Germany, 19-25 May 2007

contrast between gray and white matter in the brain, fine structures within the gray matter, such as laminar layers or cortical columns, are difficult to identify using conventional anatomical MRI. This is primarily due to the lack of significant difference in proton density, spin-lattice relaxation time (T_1), spin-spin relaxation time (T_2) and diffusion coefficients between the neural structures and their surrounding tissues. Previous attempts to identify fine cortical structures utilized T_1 contrast between gray matter and myelinated axons in gray matter to differentiate myelin-rich regions in the cortex, such as the stripe of Genari in the primary visual cortex in human (Barbier et al., 2002; Clark et al., 1992; Walters et al., 2003). Although, the resulting contrast from this method is small and the use of this approach has not found widespread application. Another study utilized proton density-weighted high resolution imaging to identify clusters of neurons in the layer II of the entorhinal cortex *ex vivo* (Augustinack et al., 2005). Again, the resolution required for this approach makes it unlikely to be used for *in vivo* studies. Recently, the use of T_2*-weighting (Li et al., 2006) or phase sensitive MRI (Duyn et al., 2007) at 7 Tesla shows promise for enabling *in vivo* visualization of laminar architecture in the gray matter due to the susceptibility differences (Marques et al., 2009).

In addition to intrinsic contrasts, cell/tissue-dependent uptake and accumulation of contrast agents can also provide a means to visualize neural structures with MRI. For example, gadolinium-based contrast agent has been demonstrated to discriminate layers in the cortex and cerebellum in perfusion fixed *ex vivo* rodent brains (Sharief and Johnson, 2006). Mn^{2+} has been demonstrated to be very useful for mapping neuronal function, connections and brain anatomy (for review, see Koretsky and Silva, 2004). A number of cytoarchitectural features in the brain, such as layers in the hippocampus, cerebral cortex, olfactory bulb, and cerebellum have also been detected with MRI *in vivo* after simple systemic administration of Mn^{2+} (Aoki et al., 2004; Silva et al., 2008; Watanabe et al., 2002). With the higher sensitivity and spatial resolution achievable at ultra-high field MRI with optimized detectors it may be possible to delineate even smaller neural units within a functional layer using manganese enhanced MRI (MEMRI).

In this study, the potential of using MEMRI to detect individual olfactory glomeruli in the rodent olfactory bulb was determined. Olfactory glomeruli are spherical neuropils located in the glomerular layer of the olfactory bulb (OB) where the axons of olfactory sensory neurons make synapses with the output neurons of the bulb called mitral cells (Mori et al., 1999). A glomerulus, consisting of input sensory neurons, projecting mitral cells, and associated inter-neurons is regarded as a fundamental information processing module in the OB (Chen and Shepherd, 2005) and is similar in size to a cortical column within layer IV of the sensory cortex. Glomeruli range from 100 to 200 microns in diameter in adult rats (Meisami and Sendera, 1993), presenting a severe challenge to visualization by MRI. Resolution of individual glomeruli by functional MRI has been described by Kida et al (2002) and Chuang et al (2009b), but discrimination by anatomical MRI has not been reported. By using Mn^{2+} as an anatomical contrast agent, T_1 weighted MRI of the rat olfactory bulb at 50 micron isotropic resolution revealed contrast changes in the glomerular layer consistent in size and shape with individual glomeruli. Contrast was detected in the living brain after systemic administration of $MnCl_2$. Potential artifacts due to blood vessels surrounding and penetrating the glomerular layer were assessed and determined not to be responsible for the contrast detected. Comparison of MRI with individual glomeruli in Nissl staining from the same olfactory bulb indicated that the MEMRI contrast correlated with glomeruli. These results indicate that high resolution MEMRI can indeed detect fundamental units of neural processing within the layers of the rodent brain as indicated by the glomeruli in the olfactory bulb.

Methods

Animal preparation

Thirteen adult male Sprague-Dawley rats (body weights 200–350 g) were used in this study. All animal work followed the guidelines of the Animal Care and Use Committee of National Institute of Neurological Disorders and Stroke, National Institutes of Heath (Bethesda, MD). For manganese enhancement, 176 mg/kg of 120-mM $MnCl_2$ (Sigma-Aldrich, St. Louis, MO) solution was infused into 10 rats via the tail vein at a rate of 2.25 mL/h by a syringe pump (Cole-Parmer Instrument, Vernon Hills, IL). During the infusion, the rats were anesthetized with 0.5–1.2 % isoflurane and their body temperatures were maintained by a warm water bath. After infusion, rats were kept on the warm water bath until fully awake and were returned to cages for free access to food and water. No abnormality was observed in these rats after recovery from the infusion.

One day after $MnCl_2$ infusion, the rats underwent MRI scans. Rats were orally intubated, connected to a mechanical ventilator (CWE SAR-830/P, Ardmore, PA), and secured in a plastic stereotaxic holder. The anesthesia, isoflurane, was kept between 1.5–2.0 % and the breathing rates and end-tidal CO_2 were carefully monitored and controlled to maintain proper cardiovascular function. The body temperature was maintained at 37°C by a temperature controlled water bath.

MRI acquisition

Images were acquired on an 11.7 T/31 cm horizontal magnet (Magnex Scientific Ltd., Abingdon, UK) interfaced to a Bruker Avance console (Bruker BioSpin, Billerica, MA). A homemade, 9-cm birdcage coil was used for homogeneous RF transmission and a double-loop, 1-cm surface coil placed on top of the OB was used for signal reception. The manganese enhanced contrast was detected by 3D T_1-weighted rapid acquisition with relaxation enhancement (RARE) sequence with TR/TE = 300/9.7 ms, matrix size = 256 × 288 × 192, RARE factor = 2, and 50-μm isotropic nominal resolution. The scan time was 2 h 20 min. Then, 3D gradient echo images (TR/TE/flip-angle = 50/3.5/25°; 50-μm isotropic resolution; scan time = 34 min) were acquired before and after intravenous injection of MION. The total scan time was less than 4 h in this experiment. Finally, to determine vascular effects in the T_1-weighted imaging, 2D T_1-weighted RARE images (TR/TE = 300/9.7 ms; RARE factor = 2; 50-μm in-plane resolution; slice thickness = 0.15 mm; average = 75) were acquired in 3 rats before and after euthanasia by overdosing with halothane.

Histology

After MRI scan, the brains of 8 rats were perfused transcardially by phosphate buffered saline (pH 7.4) and fixed in 4% paraformaldehyde. The skull was removed and the OB was carefully extracted, stored at 4°C, and sent for sectioning and histological processing (HistoServe, Rockville, MD). Serial 25-micron coronal sections of the OB were stained with Nissl. The histology sections were imaged by a Leica MZ FL III light microscope with 1.25x object (Leica Microsystems Inc., Bannockburn, IL) and a cooled CCD camera (Micropublisher 3.3, QImaging, Surrey, BC, Canada).

Data analysis

The signal-to-noise ratio (SNR) of the 3D T_1-weighted RARE image was calculated by dividing the average signal in a region-of-interest (ROI) in the OB by the standard deviation (SD) of an artifact-free region in the background. Two ROIs covering the glomerular and mitral cell layers of the OB were chosen from the dorsal and ventral parts of OB. The contrast of the signal variation in the glomerular layer was defined as the difference between a signal peak

and its adjacent trough in a line profile. The contrast-to-noise ratio (CNR) was calculated by dividing the averaged contrasts in the line profile by the SD in a background region. Line profiles of the glomerular layer were drawn in coronal sections of the T_1-weighted MRI using ImageJ (NIH, Bethesda, MD; http://rsb.info.nih.gov/ij/). In images without Mn^{2+} enhancement, the glomerular layer was identified based on the atlas (Paxinos and Watson, 1998) or the images of the same animal after Mn^{2+} infusion.

Blood vessels were identified from the MION-enhanced gradient echo images. A vascular map was created by subtracting the pre-injection with the post-injection image and dividing by the pre-injection one (Bolan et al., 2006). Line profiles of the glomerular layer at the same locations as drawn in the T_1-weighted RARE image were obtained from the vascular map and correlated with the profiles of MEMRI.

The MEMRI data was co-registered with the histology using MIPAV (NIH, Bethesda, MD; http://mipav.cit.nih.gov/) together with custom written tools in Matlab (MathWorks Inc., Natick, MA). First, the illumination inhomogeneity in the histological images was corrected by a blank reference image and the coil B_1 field inhomogeneity of the T_1-weighted MRI was corrected by the N3 algorithm (Sled et al., 1998). Then the RGB images of the histological sections were converted to grayscale and the intensity was inverted, thus the stained regions became bright and the background became dark. 3D histology stack was created by aligning the 2D histological images to the most-posterior slice using a 2D rigid-body transformation. To reduce the resolution differences between the histology and MRI, the 3D histology stack was smoothed by a Gaussian kernel with full-width-at-half-maximum of 5 times the in-plane resolution and 2 times the section thickness, and sub-sampled by a factor of 8 in both in-plane directions. Finally, the T_1-weighted image was registered to the histology stack using minimal normalized correlation and 3D affine transformation.

Results

In Fig. 1a, we show coronal sections of the T_1-weighted images acquired from a rat OB both before and after Mn^{2+} infusion. Without manganese enhancement, no contrast between the layers of the OB can be observed with the parameters used and the SNR was about 10 to 4 from the dorsal to the ventral parts of the OB at 50 μm isotropic resolution in vivo. 24 h after Mn^{2+} infusion, the SNR was increased by 50%–200% across the OB. The SNR became 27.7 ± 5.9 in the dorsal OB and 7.0 ± 1.8 in the ventral OB.

The glomerular and mitral cell layers were especially enhanced as reported previously (Aoki et al., 2004; Lee et al., 2005). With the high-resolution imaging, several round-shaped, high-intensity spots could be observed on the dorsal, medial and lateral sides of the glomerular layer (for example, the arrows in Fig. 1A). The sizes of these spots were about 2 to 4 pixels (i.e., 100 to 200 μm) in diameter, which correspond well with the known sizes of rat glomeruli of about 150 μm (Meisami and Sendera, 1993; Meister and Bonhoeffer, 2001). Line profiles were drawn along the glomerular layer in these T_1-weighted images (Fig. 1B). Compared with the SNR profile before Mn^{2+} infusion, there were several signal peaks corresponding to the identified spots in Fig. 1a. The CNRs of these signal peaks were estimated from several coronal sections. The CNR of signal peaks after Mn^{2+} infusion (4.7 ± 2.1) was significantly higher than that before infusion (2.8 ± 1.1; $p < 10^{-10}$, unpaired Student t-test). Compared to the glomerular layer, the SNR of the mitral cell layer underneath also increased with similar trend in general, but it doesn't have organized structures like those found in the glomerular layer (Fig. 1C). Therefore, the enhanced spots could represent structures particularly in the glomerular layer, such as glomeruli or artifacts from large blood vessels.

To minimize the confounding effects due to inflow enhancement of arteries and dark signal of veins, flow saturation and 100% O_2 were used during image acquisition. Comparing T_1-weighted images acquired with and without flow saturation, high signal intensity in large arteries near the surface of the OB was reduced. The signals of large venous vessels were increased by ventilating with 100% O_2 but some of the vessels still had lower signal than nearby parenchyma.

To evaluate the amount of residual vascular artifacts in the T_1-weighted image, images were acquired before and after euthanizing animals. Fig. 2 shows the images and SNR profiles in the glomerular layer acquired in a rat before and after euthanasia. The 2D image in live rat shows high signal in arteries surrounding the outer surface of the OB. But in the glomerular layer, the SNR profiles between the live and dead rat (Fig. 2b) were very similar (correlation coefficient = 0.85, 0.94, 0.79 in 3 rats, respectively). By subtracting the SNR profile of live rat by that of the dead, the difference did not show any structures that could be attributed to blood vessels. This indicates that, without manganese enhancement, the intensity variation in the glomerular layer in the T_1-weighted image was not due to blood vessels.

The relationship between the manganese-enhanced spots and blood vessels were further investigated by injecting MION as an intravascular agent (Fig. 3a). From the MION-enhanced gradient echo images, lots of blood vessels oriented radially through the layers of the OB in the coronal plane can be observed. Compared with the T_1-weighted image, some vessels correspond to boundaries of the enhanced spots indicating that these regions of higher contrast may have been created by the presence of veins (blue arrows in Fig. 3a). However, there are still many manganese-enhanced spots that do not have blood vessels nearby (red arrows in Fig. 3a).

The distribution and orientation of blood vessels can be easily visualized from the vascular map created by subtracting the MION-enhanced image from the image before injecting MION (Fig. 3b). Similar to other cortical regions in the brain, there are large vessels surrounding the outer surface of the OB with many small vessels penetrating the layers of the OB perpendicularly. The relative locations of the manganese-enhanced spots and blood vessels in the glomerular layer were evaluated by drawing line profiles along the layer (Fig. 3c). It can be seen that many of the manganese-enhanced peaks were surrounded by vessels and some even overlapped with the vessels. However, the contrast of the manganese-enhanced peaks did not correlate with the sizes of the nearby vessels, indicating that the contrast detected in MEMRI are mainly due to Mn^{2+} accumulated in the structures in the glomerular layer and not due to boundaries created by signal loss due to blood vessels.

There were many Nissl stained glomeruli that corresponded with the contrast images from the MEMRI. Fig. 4 shows the corresponding MEMRI and Nissl staining of the OBs from two rats. In the Nissl staining, individual glomeruli can be clearly identified as large round-shaped structures near the outer surface of the OB, directly beneath the olfactory nerve layer. Based on the relative distances to the grid lines and the curvature of glomerular/mitral cell layers, many of the isolated spots in the MEMRI (indicated by arrows) could be found to correspond well with the individual glomeruli in the Nissl staining, particularly those on the lateral and medial sides of the OB where glomeruli are generally larger. Although periglomerular cells, which are interneurons surrounding and innervating glomeruli, can also be enhanced by Mn^{2+}, their sizes are only a few microns and hence the observed signal would mostly come from the glomeruli. The lower SNR of the MRI on the ventral part of the OB made it difficult to determine a one-to-one correspondence with the histology. On the dorsal side of the OB, there are many small-sized glomeruli pack closely next to or on top of each other. Therefore, the lower correspondence on the dorsal part was probably due to the partial volumetric merging of several glomeruli into one structure in MEMRI (for example, the wide blob of Mn^{2+}

enhancement at the upper-right corner of the OB in Fig. 4B). In some parts of the OB, the corresponding glomerulus in the histology was also shifted slightly due to residual distortion in the histological image that couldn't be compensated by the linear registration, making it difficult to determine corresponding glomeruli.

Discussion

Using Mn^{2+} we demonstrated that individual olfactory glomeruli can be detected *in vivo* by MRI. Functional MRI (fMRI) methods have been used to distinguish activation in neural units such as ocular dominance columns, orientation columns, whisker barrels, and the glomerular layer (Cheng et al., 2001; Duong et al., 2001; Kim et al., 2000; Xu et al., 2000; Xu et al., 2003; Yang et al., 1996), including olfactory activation at the level of individual glomeruli (Kida et al., 2002). Recently, we showed that odor-induced functional connectivity into individual glomeruli in the mouse olfactory bulb can be identified (Chuang et al., 2009b). Thus, there is accumulating evidence that fMRI may be used to resolve activity in these fundamental units of neural processing. To the best of our knowledge this is the first report demonstrating the use of an anatomical based MRI technique to detect individual glomeruli or any unit smaller than a layer *in vivo*. It will be of growing importance to compare fMRI with anatomical localization of these processing units.

Traditionally, glomeruli are identified by histological staining such as Nissl, cytochrome oxidase (Meisami and Sendera, 1993), olfactory marker protein (Slotnick et al., 2001), or Sudan black (LaMantia et al., 1992). However, the tissue has to be processed *ex vivo* and distortion is introduced during the process. Glomeruli can also be detected *in vivo* by fluorescent imaging with styryl dye (LaMantia et al., 1992) or Ca^{2+} sensitive dyes (Wachowiak et al., 2004), but the field-of-view is limited to small regions on the dorsal surface of the bulb. Gene-targeting methods can be used to label glomeruli receiving projections from olfactory receptors expressing a targeted gene (Belluscio et al., 2002; Mombaerts et al., 1996) but only specific glomeruli can be highlighted in this manner. Functional optical imaging methods can be used to detect glomeruli as well (Rubin and Katz, 1999), though matching with anatomy in the same animal is usually difficult and has required genetic expression of reporter proteins (Belluscio et al., 2002; Lodovichi et al., 2003).

Using blood oxygenation level dependent fMRI at high-resolution, it was demonstrated that olfactory activation can be detected at the glomerular layer of the mouse OB (Xu et al., 2003) and potentially at single glomerular level in the rat OB (Kida et al., 2002). However, the resolvability of this technique is affected by the artifact from large draining vein, by the point spread function of the imaging method, and ultimately limited by the vasculature of the neural unit (Kim and Ogawa, 2002). Therefore, it is challenging to distinguish individual neural unit of about a hundred micron in diameter. On the contrary, as a Ca^{2+} analog, activity induced Mn^{2+} enhancement mapping could achieve better spatial specificity (Chuang et al., 2009b; Duong et al., 2000). Here we demonstrated that anatomical map of neural units could also be visualized by MEMRI. Due to the restriction of spatial resolution and SNR, the limit of spatial resolvability of MEMRI has yet to be determined. Although higher dose of Mn^{2+} may be injected to further increase the contrast, the toxicity may cause cell death (Canals et al., 2008). Besides, the tendency of Mn^{2+} to accumulate in certain regions of the brain limits its application.

Nissl staining was used to verify the detection of glomeruli in the olfactory bulb. To reduce the geometric distortion between MRI and the histology, one might image the Mn^{2+} enhanced brain after perfusion and fixation. Since Mn^{2+} is released from cells once the cells die, the Mn^{2+} enhanced contrast will become diffuse and glomeruli could not be differentiated in the *ex vivo* brain (data not shown). Alternatively, the distortion between the *in vivo* MRI and

histology can be minimized by nonlinear registration methods with manually defined landmarks (Meyer et al., 2006). Nevertheless, despite the uncertainty associated with distortion between the two modalities, MEMRI still showed many spots that corresponded well with individual glomeruli in the Nissl stained sections. In particular the larger, well dispersed glomeruli on the lateral and medial sides could readily be correlated.

The use of a small surface coil allows high SNR to be achieved within a reasonable scan time for the in vivo study of the olfactory bulb. However, the B_1 profile of a small surface coil does not have the sensitivity required for a more distant region like the ventral part of the OB. Thus, quantification of glomeruli in the entire bulb was not done. A larger cryo-coil could be used to provide better coverage with similar or higher sensitivity (Nouls et al., 2008; Ratering et al., 2008). Another approach would be to use a series of dense arrays made up of many smaller coils that should improve sensitivity from deeper areas as has been achieved in the human brain (de Zwart et al., 2004). These improvements in sensitivity could enable better differentiation of even smaller glomeruli. Finally, cardiac and respiratory gating would also be useful in reducing the potential artifacts and improving the detectability of glomeruli.

MRI was taken at about 24 hr after intravenous injection of Mn^{2+}, which is the time interval used for enhancing layers in other areas of the brain (Aoki et al., 2004; Silva et al., 2008). Mn^{2+} accumulation in the OB reaches a peak earlier than the cortex (Chuang and Koretsky, 2009), thus, it may be beneficial to determine the optimal timing for imaging the glomeruli after injection of Mn^{2+}. It may also be possible to detect glomeruli after nasal administration of Mn^{2+} which has been shown to enhance the olfactory bulb in a layer and time dependent manner (Chen et al., 2009).

In conclusion, individual olfactory glomeruli in the rodent olfactory bulb can be identified *in vivo* after systemic administration of Mn^{2+}. To the best of our knowledge, olfactory glomeruli are the smallest functional mammalian neural units that have been visualized by anatomical MRI *in vivo*. This noninvasive technique will allow longitudinal observation of the plasticity of functional neural units in development, learning, memory, degeneration, and regeneration because repeated injection of Mn^{2+} can be performed on individuals after the Mn^{2+} has cleared from the brain (Chuang et al., 2009a),.

Acknowledgments

The authors thank Nadia Bouraoud for assisting in animal procedures and Steve Dodd for MRI hardware support. This research was supported by the Intramural Research Program of the NINDS, NIH.

References

Aoki I, Wu YJ, Silva AC, Lynch RM, Koretsky AP. In vivo detection of neuroarchitecture in the rodent brain using manganese-enhanced MRI. Neuroimage 2004;22:1046–1059. [PubMed: 15219577]

Augustinack JC, van der Kouwe AJ, Blackwell ML, Salat DH, Wiggins CJ, Frosch MP, Wiggins GC, Potthast A, Wald LL, Fischl BR. Detection of entorhinal layer II using 7Tesla magnetic resonance imaging. Ann Neurol 2005;57:489–494. [PubMed: 15786476]

Barbier EL, Marrett S, Danek A, Vortmeyer A, van Gelderen P, Duyn J, Bandettini P, Grafman J, Koretsky AP. Imaging cortical anatomy by high-resolution MR at 3.0T: detection of the stripe of Gennari in visual area 17. Magn Reson Med 2002;48:735–738. [PubMed: 12353293]

Belluscio L, Lodovichi C, Feinstein P, Mombaerts P, Katz LC. Odorant receptors instruct functional circuitry in the mouse olfactory bulb. Nature 2002;419:296–300. [PubMed: 12239567]

Bolan PJ, Yacoub E, Garwood M, Ugurbil K, Harel N. In vivo micro-MRI of intracortical neurovasculature. Neuroimage 2006;32:62–69. [PubMed: 16675271]

Canals S, Beyerlein M, Keller AL, Murayama Y, Logothetis NK. Magnetic resonance imaging of cortical connectivity in vivo. Neuroimage 2008;40:458–472. [PubMed: 18222710]

Chen, DY.; Chuang, KH.; Dodd, SJ.; Koretsky, AP. In vivo Tracing of Cortical Laminar Structure in the Rodent Olfactory System using Manganese-Enhanced MRI (MEMRI). Proc Intl Soc Magn Reson Med 17th Meeting; Hawaii, USA. 2009.

Chen WR, Shepherd GM. The olfactory glomerulus: a cortical module with specific functions. J Neurocytol 2005;34:353–360. [PubMed: 16841172]

Cheng K, Waggoner RA, Tanaka K. Human ocular dominance columns as revealed by high-field functional magnetic resonance imaging. Neuron 2001;32:359–374. [PubMed: 11684004]

Chuang KH, Koretsky AP. Accounting for nonspecific enhancement in neuronal tract tracing using manganese enhanced magnetic resonance imaging. Magn Reson Imaging. 2009in press

Chuang KH, Koretsky AP, Sotak CH. Temporal Changes in the T1 and T2 Relaxation Rates (ΔR1 and ΔR2) in the Rat Brain are Consistent with the Tissue-Clearance Rates of Elemental Manganese. Magn Reson Med. 2009ain press

Chuang KH, Lee JH, Silva AC, Belluscio L, Koretsky AP. Manganese enhanced MRI reveals functional circuitry in response to odorant stimuli. Neuroimage 2009b;44:363–372. [PubMed: 18848997]

Clark VP, Courchesne E, Grafe M. In vivo myeloarchitectonic analysis of human striate and extrastriate cortex using magnetic resonance imaging. Cereb Cortex 1992;2:417–424. [PubMed: 1422094]

de Zwart JA, Ledden PJ, van Gelderen P, Bodurka J, Chu R, Duyn JH. Signal-to-noise ratio and parallel imaging performance of a 16-channel receive-only brain coil array at 3.0 Tesla. Magn Reson Med 2004;51:22–26. [PubMed: 14705041]

Duong TQ, Kim DS, Ugurbil K, Kim SG. Localized cerebral blood flow response at submillimeter columnar resolution. Proc Natl Acad Sci U S A 2001;98:10904–10909. [PubMed: 11526212]

Duong TQ, Silva AC, Lee SP, Kim SG. Functional MRI of calcium-dependent synaptic activity: cross correlation with CBF and BOLD measurements. Magn Reson Med 2000;43:383–392. [PubMed: 10725881]

Duyn JH, van Gelderen P, Li TQ, de Zwart JA, Koretsky AP, Fukunaga M. High-field MRI of brain cortical substructure based on signal phase. Proc Natl Acad Sci U S A 2007;104:11796–11801. [PubMed: 17586684]

Kida I, Xu F, Shulman RG, Hyder F. Mapping at glomerular resolution: fMRI of rat olfactory bulb. Magn Reson Med 2002;48:570–576. [PubMed: 12210928]

Kim DS, Duong TQ, Kim SG. High-resolution mapping of iso-orientation columns by fMRI. Nat Neurosci 2000;3:164–169. [PubMed: 10649572]

Kim SG, Ogawa S. Insights into new techniques for high resolution functional MRI. Curr Opin Neurobiol 2002;12:607–615. [PubMed: 12367643]

Koretsky AP, Silva AC. Manganese-enhanced magnetic resonance imaging (MEMRI). NMR Biomed 2004;17:527–531. [PubMed: 15617051]

LaMantia AS, Pomeroy SL, Purves D. Vital imaging of glomeruli in the mouse olfactory bulb. J Neurosci 1992;12:976–988. [PubMed: 1545246]

Lee JH, Silva AC, Merkle H, Koretsky AP. Manganese-enhanced magnetic resonance imaging of mouse brain after systemic administration of MnCl2: dose-dependent and temporal evolution of T1 contrast. Magn Reson Med 2005;53:640–648. [PubMed: 15723400]

Li TQ, van Gelderen P, Merkle H, Talagala L, Koretsky AP, Duyn J. Extensive heterogeneity in white matter intensity in high-resolution T-2(*)-weighted MRI of the human brain at 7.0 T. Neuroimage 2006;32:1032–1040. [PubMed: 16854600]

Lodovichi C, Belluscio L, Katz LC. Functional topography of connections linking mirror-symmetric maps in the mouse olfactory bulb. Neuron 2003;38:265–276. [PubMed: 12718860]

Marques JP, Maddage R, Mlynarik V, Gruetter R. On the origin of the MR image phase contrast: an in vivo MR microscopy study of the rat brain at 14.1 T. Neuroimage 2009;46:345–352. [PubMed: 19254768]

Meisami E, Sendera TJ. Morphometry of rat olfactory bulbs stained for cytochrome oxidase reveals that the entire population of glomeruli forms early in the neonatal period. Brain Res Dev Brain Res 1993;71:253–257.

Meister M, Bonhoeffer T. Tuning and topography in an odor map on the rat olfactory bulb. J Neurosci 2001;21:1351–1360. [PubMed: 11160406]

Meyer CR, Moffat BA, Kuszpit KK, Bland PL, McKeever PE, Johnson TD, Chenevert TL, Rehemtulla A, Ross BD. A methodology for registration of a histological slide and in vivo MRI volume based on optimizing mutual information. Mol Imaging 2006;5:16–23. [PubMed: 16779966]

Mombaerts P, Wang F, Dulac C, Chao SK, Nemes A, Mendelsohn M, Edmondson J, Axel R. Visualizing an olfactory sensory map. Cell 1996;87:675–686. [PubMed: 8929536]

Mori K, Nagao H, Yoshihara Y. The olfactory bulb: coding and processing of odor molecule information. Science 1999;286:711–715. [PubMed: 10531048]

Nouls JC, Izenson MG, Greeley HP, Johnson GA. Design of a superconducting volume coil for magnetic resonance microscopy of the mouse brain. J Magn Reson 2008;191:231–238. [PubMed: 18221901]

Paxinos, G.; Watson, C. The rat brain in stereotaxic coordinates. Vol. 4. Academic Press; 1998.

Ratering D, Baltes C, Nordmeyer-Massner J, Marek D, Rudin M. Performance of a 200-MHz cryogenic RF probe designed for MRI and MRS of the murine brain. Magn Reson Med 2008;59:1440–1447. [PubMed: 18421696]

Rubin BD, Katz LC. Optical imaging of odorant representations in the mammalian olfactory bulb. Neuron 1999;23:499–511. [PubMed: 10433262]

Sharief AA, Johnson GA. Enhanced T2 contrast for MR histology of the mouse brain. Magn Reson Med 2006;56:717–725. [PubMed: 16964618]

Silva AC, Lee JH, Wu CW, Tucciarone J, Pelled G, Aoki I, Koretsky AP. Detection of cortical laminar architecture using manganese-enhanced MRI. J Neurosci Methods 2008;167:246–257. [PubMed: 17936913]

Sled JG, Zijdenbos AP, Evans AC. A nonparametric method for automatic correction of intensity nonuniformity in MRI data. IEEE Trans Med Imaging 1998;17:87–97. [PubMed: 9617910]

Slotnick B, Bodyak N, Davis BJ. Olfactory marker protein immunohistochemistry and the anterograde transport of horseradish peroxidase as indices of damage to the olfactory epithelium. Chem Senses 2001;26:605–610. [PubMed: 11473926]

Wachowiak M, Denk W, Friedrich RW. Functional organization of sensory input to the olfactory bulb glomerulus analyzed by two-photon calcium imaging. Proc Natl Acad Sci U S A 2004;101:9097–9102. [PubMed: 15184670]

Walters NB, Egan GF, Kril JJ, Kean M, Waley P, Jenkinson M, Watson JD. In vivo identification of human cortical areas using high-resolution MRI: an approach to cerebral structure-function correlation. Proc Natl Acad Sci U S A 2003;100:2981–2986. [PubMed: 12601170]

Watanabe T, Natt O, Boretius S, Frahm J, Michaelis T. In vivo 3D MRI staining of mouse brain after subcutaneous application of MnCl2. Magn Reson Med 2002;48:852–859. [PubMed: 12418000]

Xu F, Kida I, Hyder F, Shulman RG. Assessment and discrimination of odor stimuli in rat olfactory bulb by dynamic functional MRI. Proc Natl Acad Sci U S A 2000;97:10601–10606. [PubMed: 10973488]

Xu F, Liu N, Kida I, Rothman DL, Hyder F, Shepherd GM. Odor maps of aldehydes and esters revealed by functional MRI in the glomerular layer of the mouse olfactory bulb. Proc Natl Acad Sci U S A 2003;100:11029–11034. [PubMed: 12963819]

Yang X, Hyder F, Shulman RG. Activation of single whisker barrel in rat brain localized by functional magnetic resonance imaging. Proc Natl Acad Sci U S A 1996;93:475–478. [PubMed: 8552664]

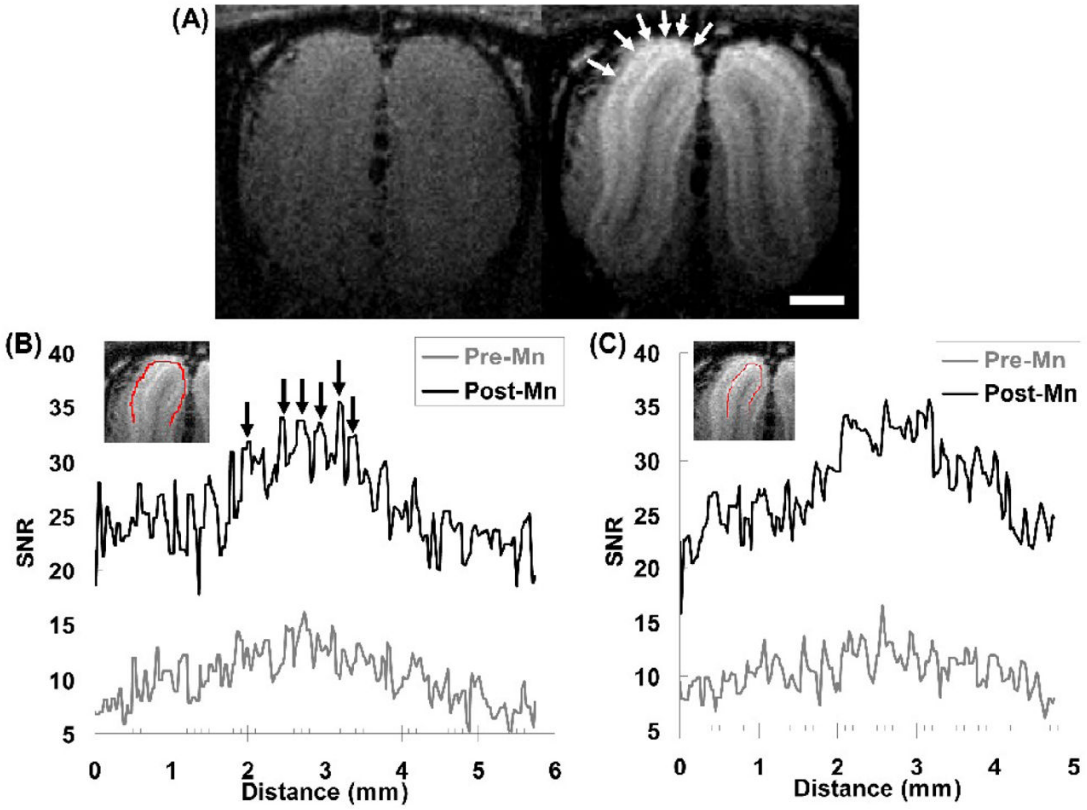

Fig. 1.

(A) Coronal sections of 3D T_1-weighted MRI of a rat before (left) and 24 h after (right) intravenous injection of $MnCl_2$. Mn^{2+} enhanced spots could be identified in the dorsal (arrows), lateral, and medial portions of the glomerular layer. The scale bar represents 1 mm. (B) The SNR profiles in the upper half of the glomerular layer (the red line in the inserted image) show significant increase in SNR after Mn^{2+} injection (noted the vertical scales of the two profiles are different). Especially higher contrast could be seen at certain locations (arrows) with widths about 100–200 microns, which correspond well with the dimensions of olfactory glomeruli. (C) The SNR profiles in the mitral cell layer (the red line in the inserted image) underneath the glomerular layer in (B) only has general increase in SNR but doesn't show organized structures.

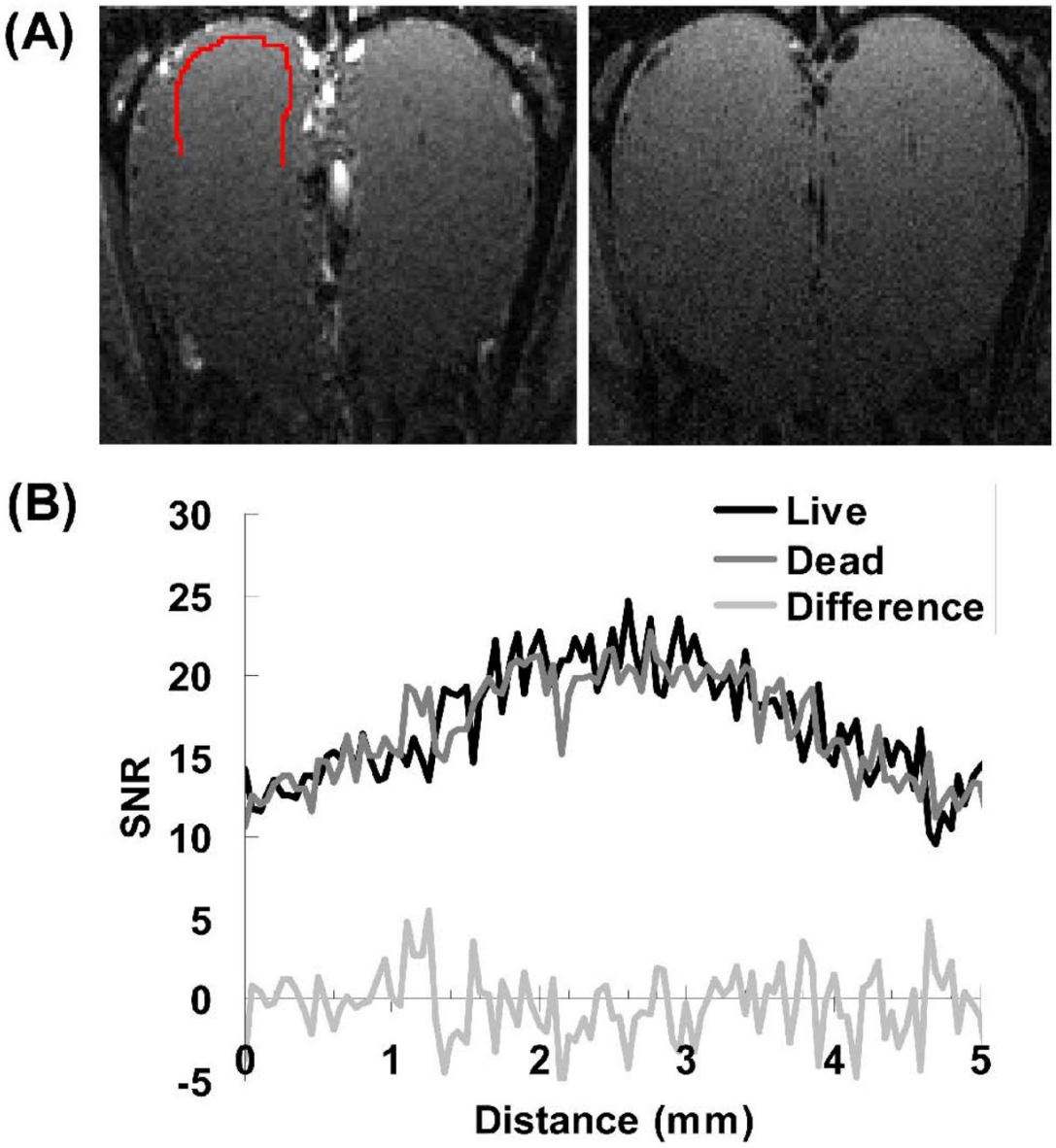

Fig. 2.

(A) T_1-weighted images of a rat before (left) and after (right) euthanasia. (B) The SNR profiles along the glomerular layer (indicated as the red curve in (A)) are similar between live (black line) and dead (gray line). Without Mn^{2+} enhancement, no distinguishable structure can be found in the difference between the two profiles (light gray line).

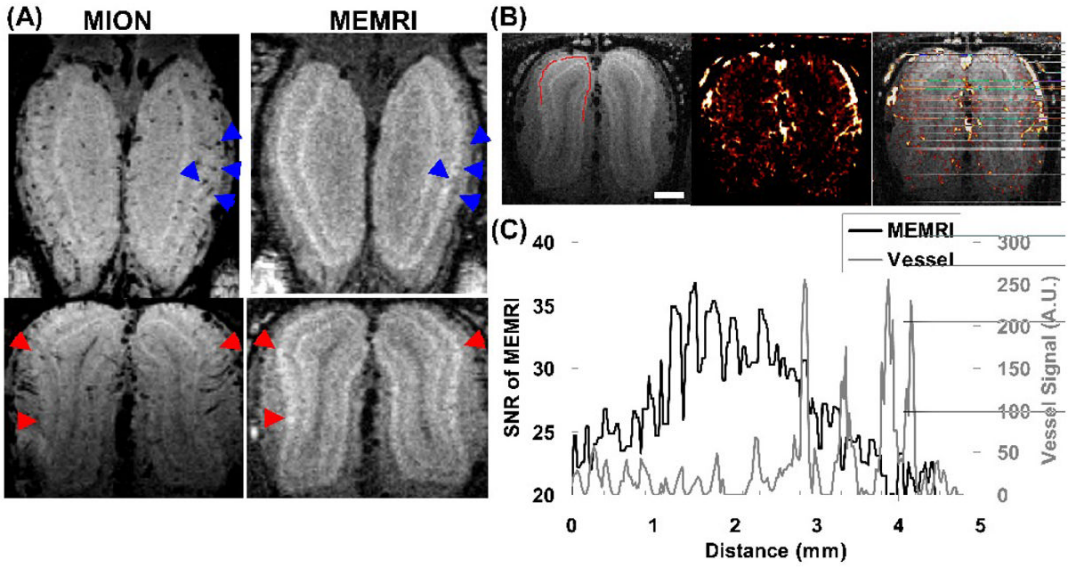

Fig. 3.

(A) Horizontal (top) and coronal (bottom) sections of the gradient echo images after injection of MION show that the boundaries at certain locations in the MEMRI (e.g., the blue arrowheads) are formed by blood vessels surrounding or penetrating the glomerular layer. However, there are also many Mn^{2+} enhanced spots (e.g., the red arrowheads) don't have visible vessels nearby. (B) Blood vessels can be delineated by subtracting the gradient echo image before MION injection by the image after injection: MEMRI (left); vessel map (middle); vessels overlaid on MEMRI (right). The scale bar represents 1mm. (C) The SNR profile of MEMRI in the glomerular layer (black line; location shown as the red line in (B)) shows that Mn^{2+} enhanced spots usually have blood vessels (gray line) in between. However, the Mn^{2+} contrast doesn't correlate with the signal change caused by MION.

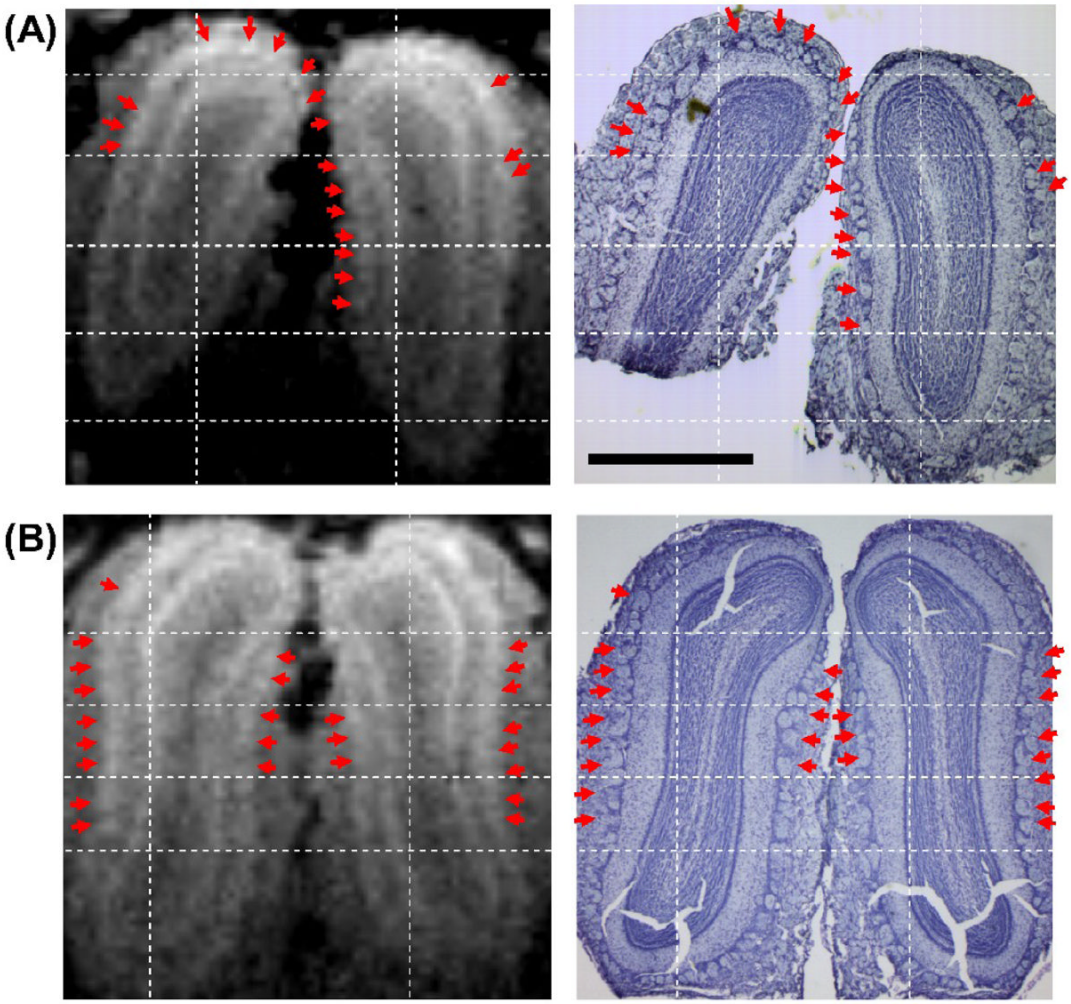

Fig. 4.
The manganese-enhanced spots (arrows) identified in MEMRI (left column) correspond well with the glomeruli shown in the Nissl staining (right column) of the same animal. A and B are the images from two rats. The scale bar represents 1 mm.